

Vibrational Spectroscopic (FT-IR and FT-Raman) Studies, HOMO LUMO Analysis and Electrostatic Potential Surface Of 2-Amino-4, 5-Dimethyl-3-Furancarbonitrile

S.Seshadri¹ Rasheed .M.P² & R.Sangeetha³

¹(Associate Professor and HOD, Department of Physics, Urumudhanalakshmi College ,Trichy-19)

²(Research Scholar, Department of Physics, Urumudhanalakshmi College ,Trichy-19)

³(Research Scholar, Department of Physics, Urumudhanalakshmi College ,Trichy-19)

Abstract: The FTIR and FT Raman spectra of 2-Amino-4,5-dimethyl-3-furancarbonitrile (ADMFC) have been recorded in the region 4000-400 cm^{-1} and 4000-100 cm^{-1} respectively. The optimized geometry, frequency and intensity of vibrational bands of 2-Amino-4,5-dimethyl-3-furancarbonitrile (ADMFC) were obtained by Density Functional Theory (DFT) using 6-311++G(d,p) basis set. The harmonic vibrational frequencies were calculated and scaled values have been compared with experimental FTIR and FT-Raman spectra. The observed and calculated frequencies are found to be in good agreement. The molecular electrostatic potential is carried out and the calculated HOMO and LUMO energies show that charge transfer occurs within the molecule. ¹H and ¹³C NMR chemical shifts were calculated with GIAO approach by applying B3LYP method. The first order hyper polarizability (β_0), related properties (β, α_0 and $\Delta\alpha$) and Mulliken charges of the molecule were also calculated using DFT calculations. Information about the charge density distribution of the molecule and its chemical reactivity has been obtained by mapping molecular electrostatic potential surface.

Key words: ADMFC, FTIR, FT Raman, HOMO, LUMO, Vibrational spectra.

I. Introduction

Furan is a heterocyclic five membered unsaturated ring compound. Furan shows aromatic properties because the resulting π molecular orbital satisfies the Huckels Rule. The furan nucleus is also found in large number of biologically active materials. Synthesis of furan co polytmers from renewable vegetables have extensive applications in the paint industry[1].Furan and its derivatives exhibit a wide range of biological activities like cytotoxic and anti tumor properties, anti spasmodic and anti feeding activities [2-5].Despite the significant role of furan and its derivatives in the field of science and technology, studies on furan derivatives are still scarce.

II. Experimental Details

The compound under investigation namely 2-Amino-4,5-dimethyl-3-furancarbonitrile (ADMFC) is purchased from Lancaster chemical company, UK, and used as such for the spectral measurements without any further purification. The room temperature Fourier Transform Infrared (FTIR) spectrum of the compound was measured with KBr pellet technique in the 4000-400 cm^{-1} region at a resolution of $\pm 1 \text{ cm}^{-1}$, using a BRUKER IFS-66V vacuum Fourier transform spectrometer equipped with a cooled Mercury Cadmium Telluride (MCT) detector.

The FT-Raman spectrum was recorded at a BRUCKER IFS-66V model interferometer equipped with an FRA -106 FT-Raman accessory. The spectrum was recorded in the 3500-100 cm^{-1} Stokes region using 1064nm line of a Nd:YAG laser for excitation operating at 200 mw power. The reported wave-numbers are expected to be accurate to within $\pm 1 \text{ cm}^{-1}$.

III. Computational Details

The quantum chemical calculation of ADMFC has been performed using the B3LYP level of theory supplemented with the standard density functional triply parameter hybrid model DFT/B3LYP. The 6-311++G(d,p) basis set have been employed using the Gaussian 09 program [8]. The optimized geometry corresponding to the minimum on the potential energy surface have been obtained by solving self consistent field equation iteratively. Harmonic vibrational wavenumbers have been calculated using analytic second derivatives to confirm the convergence to minima on the potential energy surface and to evaluate the zero-point vibrational energy [9]. These force fields obtained in Cartesian coordinates and dipole derivatives with respect to atomic displacements were extracted from the archive section of the Gaussian 09 output and transformed to a suitably defined set of internal coordinates The optimized geometrical parameters, IR intensity, Raman activity, the atomic charges, dipole moment, reduced mass, force constant and other thermodynamic parameters were

also calculated. Scaling of the force field was performed according to the SQM procedure [10,11]. using selective scaling in the natural internal coordinate representation [12,13]. Transformation of the force field and subsequent normal coordinate analysis including the least square refinement of the scale factors, calculation of the potential energy distribution (PED) and the prediction of IR and Raman intensities were done on a PC with the MOLVIB program written by Sundius [14,15]. For the plots of simulated IR and Raman spectra, pure Lorentzian band shapes were used with a bandwidth of 10 cm^{-1} . The symmetry of the molecule was also helpful in making vibrational assignments. By combining the results of the Gaussview program [16] with symmetry considerations, vibrational frequency assignments were made with a high degree of confidence. The defined local symmetry coordinates form complete set and matches quite well with the motions observed using the Gaussview program. ^1H and ^{13}C NMR chemical shifts were calculated with GIAO approach [17,18] by applying B3LYP method [19,20].

IV. Prediction Of Raman Intensities

The Raman activities (S_i) calculated with the GAUSSIAN 09 program and adjusted during the scaling procedure with MOLVIB were subsequently converted to relative Raman intensities (I_i) using the following relationship derived from the basic theory of Raman scattering [21-22]

$$I_i = \frac{f(v_o - v_i)^4 S_i}{v_i \left[1 - \exp\left(\frac{-hcv_i}{kT}\right) \right]}$$

Where v_o is the exciting frequency (in cm^{-1} units); v_i is the vibrational wave number of the of the i^{th} normal mode, h , c and k are fundamental constants and f is a suitably chosen common normalization factor for all peak intensities.

V. Results And Discussion

5.1 Molecular Geometry

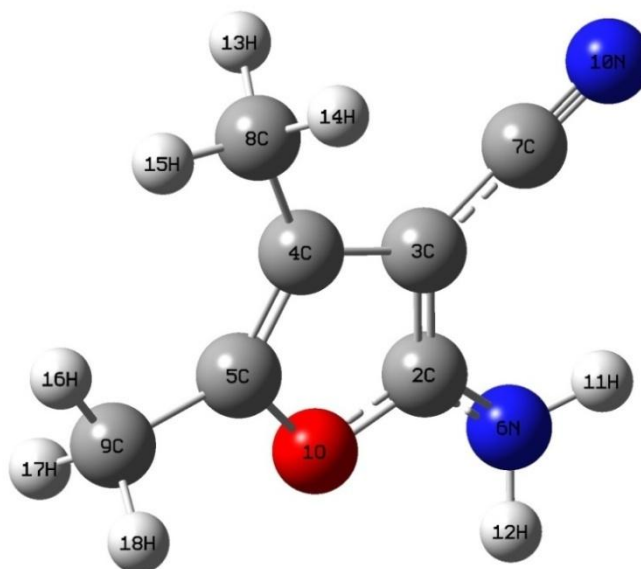


Fig 1: Structure of ADMFC along with numbering of atoms

The labeling of atoms of the title compound is shown in Figure 1. The global minimum energies obtained by the DFT structure optimization for ADMFC for B3LYP/6-31G(d,p), B3LYP/6-31+G(d,p), and B3LYP/6-311G++(d,p) basis sets respectively are presented in TABLE 1. The optimized geometrical parameters are presented in TABLE 2. This energy difference is clearly understandable, since the molecules are under different environments. The zero point vibrational energies, rotational constants, entropies and dipole moments obtained for optimized geometry with B3LYP/6-311G++(d,p) basis set are presented in TABLE 3.

TABLE 1: Total energies (in Hartrees) based on B3LYP/6-31++g(d,p) , B3LYP/6-311 + G(d,p) and B3LYP/6-311 + +G(d,p) basis sets for ADMFC

Basis set	2-Amino-4,5-dimethyl-3-furancarboxitrile
B3LYP/6-31 G(d,p)	-456.229312
B3LYP/6-311 + G(d,p)	-456.3464473
B3LYP/6-311 + +G(d,p)	-456.346456

ADMFC belongs to C_1 point group symmetry with 18 atoms composing the structure. The molecule has 48 fundamental modes of vibration. From the structural point of view of the molecule ADMFC has

$$\Gamma_{\text{vib}} = 33 A'(\text{in-plane}) + 15 A''(\text{out-of-plane}) \text{ vibrations.}$$

TABLE 2: Optimized Geometrical Parameters Of ADMFC Obtained By B3LYP/6-311 ++ G(D,P) Density Functional Calculations

Bond length	Value(Å)	Bond angle	Value(°)	Torsional angle	Value(°)
N6-H11	1.010638	C4-C5-O1	109.71	H11-N6-C2-C3	-18.8
N6-H12	1.010854	H11-N6-C2	114.93	H12-N6-C2-C3	-155.09
C8-H13	1.095704	H12-N6-H11	114.26	H13-C8-C4-C5	-239.74
C8-H14	1.092689	H13-C8-H15	106.96	H14-C8-C4-C5	-0.23
C8-H15	1.095726	H14-C8-H13	107.93	H15-C8-C4-C5	-120.74
C9-H16	1.092037	H15-C8-H14	107.93	H16-C9-C5-C4	-0.18
C9-H17	1.096418	H16-C9-H18	107.97	H17-C9-C5-C4	-120
C9-H18	1.096556	H17-C9-H16	107.99	H18-C9-C5-C4	-240.38
N10-C7	1.166959	H18-C9-H17	107.49	N10-C7-C3-C2	13.25
C5-C4	1.356548	N10-C7-C3	178.75	C4-C5-O1-C2	-0.12
C3-C2	1.379333	C3-C2-O1	110.42	C3-C2-O1-C5	-0.08
C7-C3	1.411820	C7-C3-C4	128.67	C7-C2-C4-C3	0.76
N6-C2	1.367992	N6-C2-O1	117.04	N6-C3-O1-C2	2.76
O1-C2	1.345115	C2-O1-C5	107.62	C9-C4-O1-C5	0.1
C9-C5	1.485666	C9-C5-O1	115.31	C8-C5-C3-C4	0.21
O1-C5	1.401715	C8-C4-C3	125.09		
C8-C4	1.496298				

For numbering of atoms refer Fig. 1.

Root mean square value is obtained in the study using the following expression

$$\text{RMS} = \sqrt{\frac{1}{n-1} \sum_i^n (v_i^{\text{calcu}} - v_i^{\text{exp}})^2}$$

The RMS error between unscaled (B3LYP/6-311++G(d,p)) and experimental frequencies is found to be 50.7 cm^{-1} . This is quite obvious since the frequencies calculated on the basis of quantum mechanical force fields usually differ appreciably from observed frequencies. This is partly due to the neglect of anharmonicity and partly due to the approximate nature of the quantum mechanical methods. In order to reproduce the observed frequencies, refinement of scaling factors are applied and optimized via least square refinement algorithm which resulted in a weighted RMS deviation of 9.75 cm^{-1} between the experimental and scaled frequencies.

5.2 Assignment Of Spectra

Detailed description of vibrational modes can be given by means of normal coordinate analysis. The observed and calculated frequencies, calculated IR, Raman and normal mode descriptions (characterized by PED) are reported in TABLE 4 for ADMFC. The observed and simulated FT-IR and FT-Raman spectra of ADMFC are presented in Figure 2 and Figure 3 respectively. When using computational methods to predict theoretical normal vibrations for relatively complex poly atomics, scaling strategies are used to bring computed wave numbers into closer agreement with observed frequencies using the latest version of MOLVIB program . For ADMFC, a multiple scale factors are applied in the normal coordinate analysis and the subsequent least square fit refinement, results into the very close agreement between the observed fundamentals and the scaled frequencies (Table 4). Refinement of the scaling factor applied in this study achieved a weighted mean deviation of 4.27 cm^{-1} between the experimental and SQM frequencies[23-25]. It is convenient to discuss the vibrational spectra of ADMFC in terms of characteristic spectral regions as described below.

TABLE 3 : The calculated Thermodynamical parameters of ADMFC

Parameters	B3LYP/6-311++ G(d,p)
Total Energy (Thermal) E_{Total} (KCal/Mol)	95.056
Heat Capacity at constant Volume C_v (Cal/Mol-Kelvin)	37.283
Entropy S (Cal/Mol-Kelvin)	98.192
Vibrational Energy E_{vib} (KCal/Mol)	93.279
Zero-point vibrational energy (Joules/Mol)	370558.4
Rotational constants (GHZ):	A 1.8595103
	B 1.1246245
	C 0.7123078
Dipole moment (Debye):	μ_x -4.4369
	μ_y -2.1782
	μ_z 1.0258
	μ_{Total} 5.0481

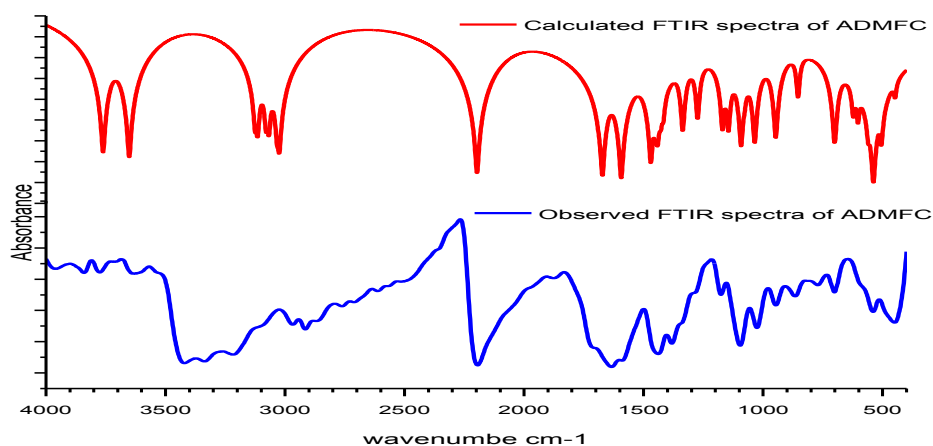


Fig 2. Comparison of Theoretical and experimental FT-IR spectrum of ADMFC

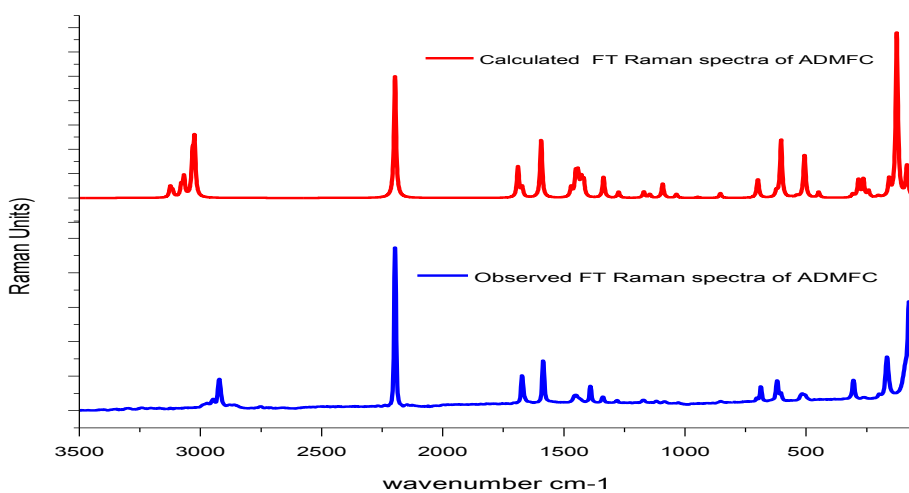


Fig 3. Comparison of Theoretical and experimental FT-Raman spectrum of ADMFC

TABLE 4: Assignment of fundamental vibrations of

No	symmetry species	Observed frequency		Calculated using B3LYP/6-311++G(d,p) force field					Characterisation of normal modes with PED%
		IR (cm ⁻¹)	Raman (cm ⁻¹)	Unscaled (cm ⁻¹)	Scale d (cm ⁻¹)	IR intensity (K mol ⁻¹)	Raman activity	Raman intensity	
1	A ^g	-	75.6	99.4	81	2.5386	0.07	367.2302	tCH3(61), gCC(31)
2	A ^g	-	-	120.2	86	6.0736	4.282	15345.2	gCC(49), tCH3(44)
3	A ^g	-	-	122	119	0.1046	0.386	1344.803	tCH3(72), gCC(14)
4	A ^g	-	-	148.3	122	0.0318	0.434	1013.723	bCCC (63), lbCCN(27)
5	A ^g	-	166.3	175	155	8.2601	0.537	894.2091	tring(61), gCC (33)
6	A ^g	-	-	236.1	199	4.2118	0.07	62.8185	gCC (77), tring(12)
7	A ^g	-	-	261	242	3.6988	0.395	288.4168	tCN (58)
8	A ^g	-	-	267	269	15.561	1.551	1079.448	bOC (61), bCC(16), tCN(11)
9	A ^g	-	-	299.9	277	14.038	2.245	1226.603	bCC(27), bOCN (18), tCN(19)
10	A ^g	-	304.7	344.2	304	4.9418	0.569	232.8467	tring (64), gCC(25),
11	A ^g	449	-	440.3	449	1.1739	1.069	259.9288	lbCCN(29), bCC (19), bOC (14)
12	A ^g	-	515.9	495.9	503	153.09	6.456	1216.609	vCC(25), bring (20), tring(15)
13	A ^g	539.8	-	513.2	505	139.23	2.366	414.0251	tring(52), gCC(38), lbCCN(6)
14	A ^g	-	-	533.9	541	3.7364	2.523	405.4746	gCN(36), bCNH(22), bHNN(14)
15	A ^g	-	-	606	571	3.6474	11.27	1374.927	lbCCN(53), gCC(20), tring(18)
16	A ^g	-	619.7	619	602	0.8429	8.582	999.6502	vCC(52), bring(13), vOC(11)
17	A ^g	-	-	629.8	621	2.9815	1.684	188.8665	bCCC(23), lbCCN(21)
18	A ^g	-	686.8	694.5	697	5.0935	6.822	616.7212	vCC(41), bring (33), tring(12)
19	A ^g	701.4	-	711.5	703	7.8822	1.612	138.1587	tring(66), gCN(27)
20	A ^g	866.6	-	860.5	853	0.7407	3.063	171.3825	vCC(37), vOC(19), vCN(12)
21	A ^g	946.6	-	952.9	949	12.857	0.725	32.1337	vOC(40), bCCH(23), vCC(13),
22	A ^g	1025.9	-	1038.3	1033	13.62	3.879	140.9512	vOC(47), bCCH(18), vCC(11)
23	A ^g	1096.1	-	1056.2	1086	0.7859	0.238	8.3053	bCCH(76), bHCH(19)
24	A ^g	-	-	1067.6	1089	0.0002	0.078	2.6693	bCCH(73), bHCH(19)
25	A ^g	-	-	1103.2	1091	29.372	4.775	150.5338	vCC (36), vOC(23), bCCH (16)
26	A ^g	1171.1	-	1135.6	1150	20.449	8.585	252.8172	bCCH(42), bHCH(15), vOC(13)
27	A ^g	-	1172	1180	1172	16.987	7.461	200.5904	vCC(45), bCCH(15),
28	A ^g	-	1280.2	1293.4	1276	5.5488	8.891	191.7767	vCC(43), vOC(15), bCNH(13)
29	A ^g	-	1339	1348.5	1333	7.8992	27.29	531.8736	vCC(43), vOC (15), bring(14)
30	A ^g	-	1390.6	1419.5	1394	4.2303	24.95	428.7471	bHCH(84), bCCH(16)
31	A ^g	-	-	1428.1	1404	2.5538	11.82	200.1613	bHCH(82), bCCH(16)
32	A ^g	-	-	1463.5	1404	84.107	9.592	152.8383	bHCH(60), bCCH(15)
33	A ^g	1439	-	1472.9	1408	5.1583	7.934	124.4124	bHCH(62), bCCH(26), vCC(11)
34	A ^g	-	-	1483.2	1418	9.6124	9.018	139.0008	bHCH(52), bCCH(33), vCC(13)
35	A ^g	-	1452.1	1493.6	1425	21.469	31.97	484.241	bHCH(48), bCCH(45)
36	A ^g	-	-	1495.9	1452	1.6293	9.893	149.262	vCC(35), vCN(13), vOC(11),

37	A'	1590.2	-	1609.8	1597	61.49	39.98	501.502 8	ν CC(62), ν CN(14)
38	A'	-	1672.3	1672.8	1671	342.87	51	580.080 2	bHNNH (55), bCNH (22), ν CN(13)
39	A'	-	-	1695.1	1692	1.3992	60.7	667.275 5	ν CC(83)
40	A'	-	2196.7	2306.5	2197	142.74	338.2	1622.65 4	ν CN(84), ν CC(16)
41	A'	-	-	3020.5	3171	43.639	336.1	720.328 6	ν CHMEL(100)
42	A'	-	-	3028.7	3179	22.021	230.3	489.408 7	ν CHMEL(100)
43	A'	-	-	3063.8	3222	15.878	132.5	271.349	ν CHMEL(100)
44	A'	-	-	3075.1	3233	11.895	75.45	152.751 7	ν CHMEL(100)
45	A'	3216	-	3110.3	3270	17.323	45.35	88.5286	ν CHMEL(100)
46	A'	3337	-	3120.4	3280	11.841	73.69	142.339 5	ν CHMEL(100)
47	A'	3421	-	3574.2	3477	61.284	192.7	236.350 1	ν NH(100)
48	A'	3638	-	3681.1	3581	46.638	50.26	55.5958	ν NH(100)

ADMFC by normal mode analysis based on SQM force field calculations using selective scaled B3LYP/6-311++g(d,p)

(ν) stretching; (b) bending; (g) scissoring and wagging ; (t) torsion
PED values greater than 10% are given

5.2.1 N-H Vibrations

The N–H stretching modes of secondary amides are generally observed in the region of 3500–3300 cm^{-1} for N–H stretching and a weak band at 3100–3070 cm^{-1} for an overtone of the N–H band [26]. For the title compound, the very strong band observed at 3421 cm^{-1} in the IR spectrum is assigned as N-H stretching mode. The calculated wavenumber for this mode is at 3574 cm^{-1} in B3LYP method. This mode is a pure stretching mode, and as it is evident from the PED column they are almost contributing 100%. The wavenumber (3574 cm^{-1}) computed by B3LYP/6-311++G(d,p) method shows the deviation (153 cm^{-1}) when compared with experimental IR data (3421 cm^{-1}). This may be due to intermolecular hydrogen bonds in solid state between the NH group and the furan N atom. This is the reason for the downshift of NH band at 3421 cm^{-1} .

The weak N–H in-plane bending mode observed at 1672 cm^{-1} in FT-Raman spectrum. The calculated wavenumber for this mode is at 1609 cm^{-1} at B3LYP method and it is scaled to 1671 cm^{-1} . Theoretically predicted values are coinciding very well with the observed frequencies. The TED corresponding to this vibration suggests that it (mode.No.38) is a medium mode and exactly contributing to 55% (Table 4).

5.2.2 CH₃ Vibration

Two asymmetric and one symmetric stretching vibrations of CH₃ group are usually observed in the range 2990–3050 cm^{-1} [27,28]. In the present case of our molecule, there were two CH₃ groups. The asymmetric stretching vibrations of CH₃ group have been identified at 3020, 3029, 3064 and 3075 cm^{-1} by B3LYP method. The asymmetric stretching vibrations of CH₃ group have been identified at 3110 and 3120 cm^{-1} in DFT method. Asymmetric stretching bands observed in the FTIR spectrum of methyl group at 3216 and 3337 cm^{-1} . The in-plane bending vibration of the CH₃ group is identified at 1439 cm^{-1} in FTIR spectrum and 1452 cm^{-1} in FT-Raman spectrum. The computed wavenumbers at 1456 cm^{-1} in B3LYP method is assigned to in-plane bending of the CH₃ group. The assignment of the band at 76 cm^{-1} of FT-Raman is attributed to the torsion CH₃ (tCH₃).

5.2.3 C–N Vibrations

The identification of C–N stretching vibrations is a very difficult task, since the mixing of several bands is possible in this region. However, with the help of the animation option of Gauss View 3.0 graphical interface for Gaussian programs and PED value from MOLVIB program, the C–N stretching vibrations are identified and assigned in this study. The C–N stretching vibrations are always mixed with other bands and normally occur in the region 1266–1382 cm^{-1} [30,31]. In our study the C–N stretching vibration observed at 1280 and 1339 cm^{-1} in FT-Raman spectrum. This vibration theoretically calculated at 1293 and 1348 cm^{-1} in B3LYP method shows good agreement with experimental findings. The assignment of the band at 261 cm^{-1} of calculated frequency is attributed to the torsion CN (tCN).

5.2.4 C - O Vibrations

The C-O stretching band of the Cyclic ethers (five membered ring) in IR spectrum is characterized by the frequencies around 920-950 cm^{-1} for C-O symmetric stretching vibration and 1060-1080 for C-O asymmetric stretching vibration. While the band in Raman spectrum usually presents a weak activity in the region of 1310 – 1210 cm^{-1} . In our case C-O stretching vibration observed at 947 cm^{-1} for symmetric stretching vibration and 1026 cm^{-1} for asymmetric stretching vibration in FT-Raman spectrum. The computed wavenumbers at 953 cm^{-1} and 1038 cm^{-1} in B3LYP method are assigned to C-O symmetric stretching vibration and C-O asymmetric stretching vibrations respectively. The PED corresponding to these vibrations suggest that they were a medium modes and exactly contributing to 40% and 47% respectively. The theoretically predicted wavenumber at 267 cm^{-1} in B3LYP method are assigned to C-C-O (bOC) in-plane mode.

5.3 Frontier Molecular Orbitals

Many organic molecules that contain conjugated π -electrons are characterized as hyperpolarizabilities and are analyzed by means of vibrational spectroscopy [32,33]. Both the Highest Occupied Molecular Orbital (HOMO) and the Lowest Unoccupied Molecular Orbital (LUMO) are the main orbital taking part in chemical reaction. The HOMO energy characterizes the ability of electron giving, the LUMO characterizes the ability of electron accepting, and the gap between HOMO and LUMO characterizes the molecular chemical stability [34]. The energy gap between the HOMOs and LUMOs called as energy gap is a critical parameter in determining molecular electrical transport properties because it is a measure of electron conductivity [35]. Surfaces for the frontier orbital's were drawn to understand the bonding scheme of present compound. The features of these MO can be seen in Figure 4.

This electronic absorption corresponds to the transition from the ground state to the first excited state and is mainly described by one electron excitation from HOMO to LUMO. While the energy of the HOMO is directly related to the ionization potential, LUMO energy is directly related to the electron affinity.

There are lots of applications available for the use of HOMO and LUMO energy gap as a quantum chemical descriptor. It establishes correlation in various chemical and bio-chemical systems [36]. The HOMO–LUMO energy gap is an important value for stability index. A large HOMO–LUMO gap implies high stability for the molecule in the sense of its lower reactivity in chemical reactions [37]. According to B3LYP/6-311++G(d,p) calculation, the energy band gap (translation from HOMO to LUMO) of the molecule is about 5.19357 eV

$$\text{HOMO energy} = - 5.80555 \text{ eV}$$

$$\text{LUMO energy} = - 0.61198 \text{ eV}$$

$$\text{HOMO-LUMO energy gap} = 5.19357 \text{ eV}$$

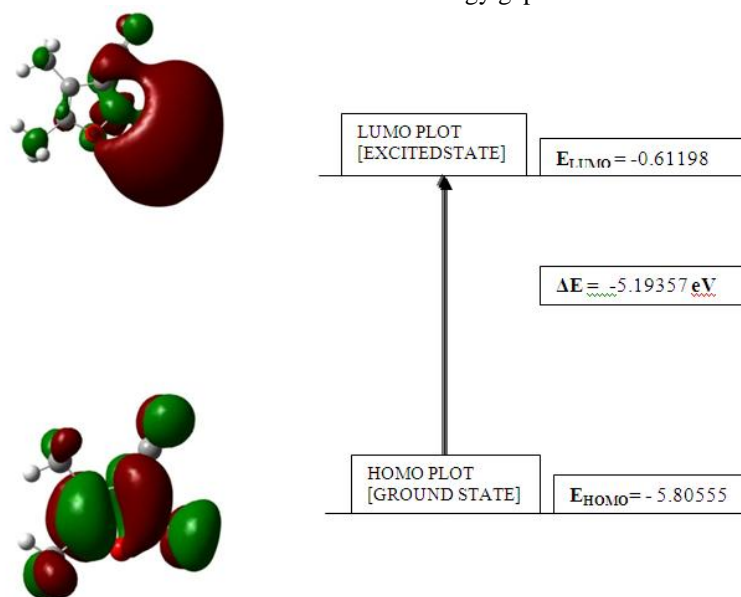


Fig 4. HOMO LUMO plot of of ADMFC

5.4. ^{13}C And ^1H NMR Spectral Analysis

Recently, Gauge Invariant Atomic Orbital's (GIAO) NMR DFT calculations have become popular [38] and can successfully predict the chemical shift (d, ppm) for small isolated molecules [39-41]. However, the accuracy of NMR theoretical predictions depend on the implemented basis set, and optimized structural parameters. Earlier investigations favor DFT predictions over the RHF method [42]. Therefore, structural

parameters obtained with the hybrid B3LYP functional at the 6-311+G(d,p) level of theory were used to predict ^1H and ^{13}C chemical shifts utilizing the recommended GIAO approach [43]. The theoretically computed ^{13}C and ^1H NMR spectrum are shown in Figure 5. Chemical shifts were reported in parts per million relative to TMS. Relative chemical shifts were estimated by using the corresponding TMS shielding calculated in advance at the same theoretical level as the reference. Aromatic carbons give signals in overlapped areas of the spectrum with chemical shift values from 100 to 150 ppm [44,45]. It can be seen from Table 6, that due to the influence of electronegative nitrogen atom, the chemical shift value of carbon atoms are significantly differing the shift positions in the range 150–180 ppm. Thus, the C2 atom has its chemical shifts at 175.85ppm. The chemical shift values of H atoms in methyl group are quite low (≤ 3 ppm) due to the shielding effect. The chemical shift values of H atoms are reported in TABLE 5.

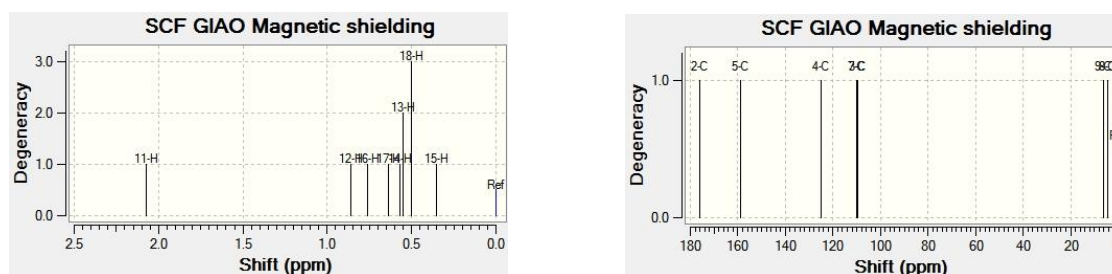


Fig 5. Theoretically calculated NMR Spectrum of ^1H and ^{13}C ADMFC

TABLE 5: Theoretical isotropic chemical shift calculated using DFT B3LYP/6-311++G(d,p) (with respect to TMS, All values in ppm) for ADMFC

Calculated chemical shift (ppm)	
Atom	B3LYP/6-311++G(d,p)
C2	175.85
C3	109.69
C4	124.93
C5	159.07
C7	110.21
C8	4.26
C9	6.28
H11	2.07
H12	0.86
H13	0.55
H14	0.57
H15	0.36
H16	0.76
H17	0.64
H18	0.5

5.5 Mulliken Charges

Mulliken atomic charge calculation [46] has an important role in the application of quantum chemical calculation to molecular system. The atomic charge in molecules is fundamental to chemistry. For instance, atomic charge has been used to describe the processes of electronegativity equalization and charge transfer in chemical reactions [47,48], and to model the electrostatic potential outside molecular surfaces [49-51]. Mulliken atomic charges calculated at the B3LYP/6-311++G(d,p) is collected in TABLE 6 along with the natural atomic charges obtained in NBO analysis. The result shows that substitution of the furan ring by oxygen leads to a redistribution of electron density. The H11 and H12 atom of ADMFC can accommodate higher positive charge and become more acidic comparing to other hydrogen atoms which have acquired a lesser positive charge. The charge on the N6 atom is less negative than N10 atom. The presence of net positive charge on H11 atom may suggest the formation of intra-molecular interaction between H11 and N10 atoms. The hydrogen is attached directly to one of the most electronegative elements, causing the hydrogen to acquire a significant amount of positive charge. Similarly the C3 atom has a higher positive charge compare to C4 atom. Because lone pairs at higher levels are more diffuse and not so attractive to positive things. Illustration of atomic charges plotted at 6-311++G(d,p) level has been shown in Figure 6.

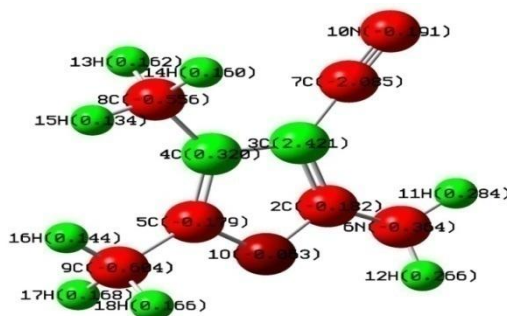


Fig 6. Illustration of mulliken atomic charges of ADMFC

TABLE 6: Atomic charges for optimized geometry of ADMFC using DFT B3LYP/6-311++g(d,p)

Atomic Number	2-Amino-4,5-dimethyl-3-furancarboxonitrile	
	Mulliken atomic charges	Natural atomic charges
C2	-0.181733	0.51886
C3	2.421038	-0.25115
C4	0.319828	-0.08712
C5	-0.178677	0.30229
C7	-2.085298	0.29679
C8	-0.555827	-0.57853
C9	-0.6036	-0.6001
H11	0.283808	0.38018
H12	0.26604	0.37417
H13	0.161906	0.21952
H14	0.159872	0.21373
H15	0.133617	0.2082
H16	0.143848	0.21681
H17	0.167828	0.22105
H18	0.165503	0.216

5.6 UV-Vis Spectral Analysis

Ultra violet spectral analysis of ADMFC has been investigated by TD-DFT/B3LYP/6-311++g(d,p) method. Calculations of molecular orbital geometry show that the visible absorption maxima of this molecule corresponds to the electron transition from HOMO to LUMO [52]. the absorption band at 223.38 is caused by $\pi \rightarrow \pi^*$ transition. The absorption bands at the longer wave lengths 256.55 and 242.48 nm of ADMFC are caused by $n \rightarrow \pi^*$ transition. The λ_{\max} is a function of substitution, the stronger the donor character substitution the more electrons pushed into the molecules, the larger the λ_{\max} . These values may be slightly shifted by solvent effects. The role of substituent and of the solvent influence on the UV Spectrum [53]. The theoretical electronic excitation energies wavelength of the excitation and oscillator strengths were calculated and listed in TABLE 7.

TABLE 7: Theoretical electronic absorption spectra values of ADMFC

Excited State	Energy (eV)	Wavelength λ (nm)	oscillator-strengths (f)
Excited State:1	4.8328	256.55	0.0806
Excited State:2	5.1132	242.48	0.001
Excited State:3	5.5503	223.38	0.0044
Excited State:4	5.7209	216.72	0.0188
Excited State:5	5.8713	211.17	0.0075
Excited State:6	6.1164	202.71	0.0048

5.7 Analysis of Molecular Electrostatic Surface Potential

The molecular electrostatic surface potential provides a visual method to understand the relative polarity of compounds[54]. Electrostatic potential map shown in Figure 7 illustrates the charge distributions of the molecule three dimensionally. The electrostatic potential generated in space by charge distribution is helpful to understand the electrophilic and nucleophilic regions in the title molecule. Knowledge of the charge distributions can be used to determine how molecules interact with one another. One of the purposes of finding the electrostatic potential is to find the reactive site of a molecule [55,56]. In the electrostatic potential map, the semispherical blue shapes that emerge from the edges of the above electrostatic potential map are hydrogen atoms. The molecular electrostatic potential (MEP) at a point r in the space around a molecule (in atomic units) can be expressed as

$$V(r) = \sum_A \frac{Z_A}{|\vec{R}_A - \vec{r}|} - \int \frac{\rho(\vec{r}')}{|\vec{r}' - \vec{r}|} d\vec{r}'$$

Where Z_A is the charge of nucleus A located at R_A , $\rho(\vec{r}')$ is the electronic density function of the molecule, and \vec{r}' is the dummy integration variable
 The first and second term represent the contributions to the potential due to nuclei and electron respectively. $V(r)$ is the net resultant electrostatic effect produced at the point r by both the electrons and nuclei of the molecule.

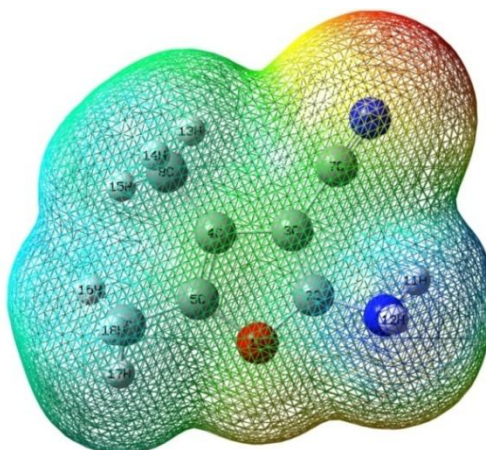


Fig 7. Total electron density isosurface mapped with molecular electrostatic potential of ADMFC

The MESP mapped surface of the compound and projection of this surface along the molecule and perpendicular plane are shown in Figure 7 and Figure 8. These figures illustrate an electrostatic potential model of the compound computed at the 0.002a.u. isodensity surface. The electrostatic potential contour map of positive and negative potential is shown in Figure 9.

Molecular electrostatic surface potential (MESP) at a point in a space around a molecule gives an indication of the net electrostatic effect produced at that point by total charge distribution (electron +nuclei) of the molecule and correlates with dipole moments, electro negativity, partial charges and chemical reactivity of the molecule. Potential increases in the following order. Red < yellow < green < blue. That is negative region (blue and yellow) are related to electrophilic reactivity. The maximum positive regions are localized on the furan ring which can be considered as possible sites for nucleophilic attack. That is negative potential sites are on the electronegative atoms while the positive potential sites around the hydrogen and carbon atom. Green area covers parts of the molecule where electrostatic potentials are nearly equal to zero (C-C bond). This is a region of zero potential enveloping the π systems of aromatic ring leaving a more electrophilic region in the plane of hydrogen atom.

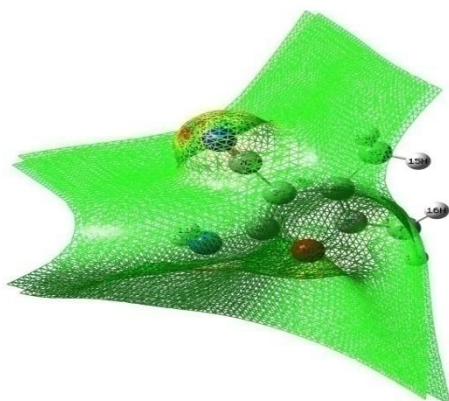


Fig 8 The electrostatic potential surface

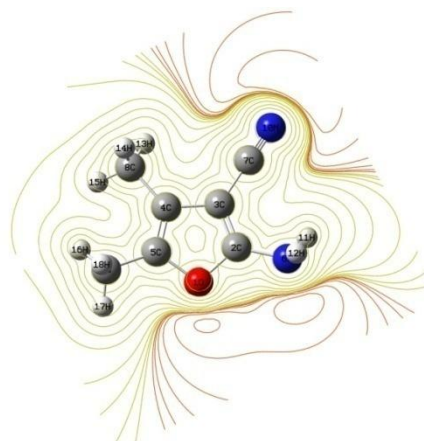


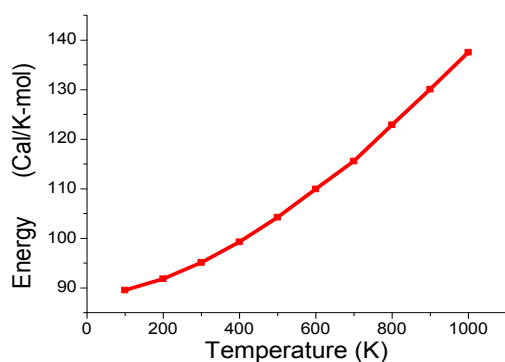
Fig 9: Contour map of molecular electrostatic potential surface

VI. Thermodynamic Analysis

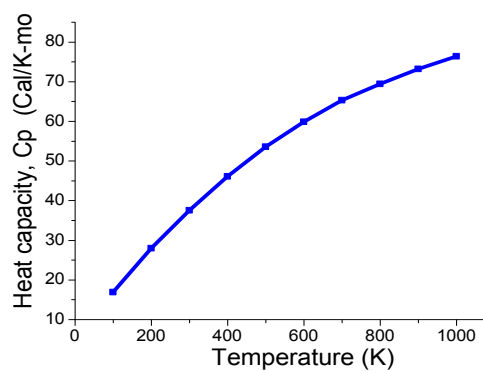
The molecule taken for this investigation has a great deal of interest in thermodynamic property analysis. Based on the vibrational analysis of title molecule at B3LYP/6-311++ G(d,p) basis set The thermodynamic parameters such as heat capacity at constant volume (C_V), Entropy (S), enthalpy change (ΔH) were calculated for different temperatures and listed in the TABLE 8. From Figures 10-13 depict the correlation of heat capacity at constant volume (C_V), Entropy (S), enthalpy (ΔH) with temperature. While performing DFT Calculations the molecule was considered to be at room temperature (298.15K) and at a pressure of 1atm. Due to increase in vibrational intensities the entropies, heat capacities and enthalpy change are increasing with temperature ranging from 100K to 1000K. The entropy and enthalpy changes revealed that the molecule possesses more flexibility of changing its own thermodynamic system with respect to the temperature.

TABLE 8: The Temperature dependence of Thermodynamic parameters of ADMFC

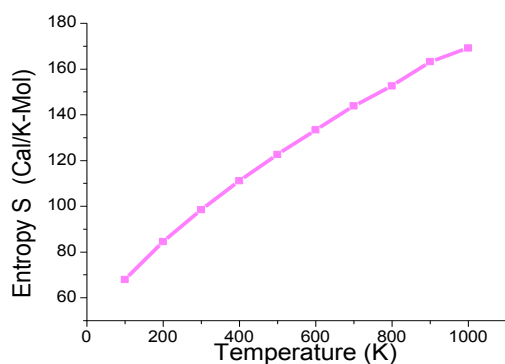
Temperature (K)	Energy (Cal/K-mol)	Heat capacity, Cp (Cal/K-mol)	Entropy S (Cal/K-Mol)	Enthalpy change (kJ/ mol)
100	89.504	16.848	67.904	0.140232
200	91.763	27.936	84.497	0.147321
300	95.04	37.478	98.467	0.152408
400	99.228	46.084	111.023	0.159397
500	104.219	53.54	122.574	0.167668
600	109.896	59.797	133.268	0.17703
700	115.509	65.323	143.732	0.186292
800	122.872	69.414	152.493	0.198343
900	130.005	73.143	163.07	0.210027
1000	137.483	76.332	169.155	0.22226



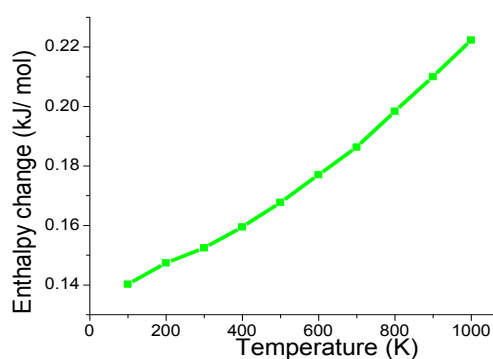
—■— Fig. 10



—■— Fig. 11



—■— Fig. 12



—■— Fig. 13

Fig 10: Temperature dependence of Energy ADMFC

Fig 11: Temperature dependence of Heat Capacity At Constant Pressure of ADMFC

Fig 12: Temperature dependence of Entropy of ADMFC

Fig 13: Temperature dependence of Enthalpy Change of ADMFC

VII. Hyperpolarizability

The first hyperpolarizability and related properties of ADMFC are calculated by B3LYP/6-311++G(d,p) basis set, based on the finite field approach. In the presence of an applied electric field, the energy of a system is a function of electric field. First hyper polarizability is a third rank tensor can be described by a 3x3 matrix. The 27 components of the 3D matrix can be reduced to 10 components due to the Kleinman symmetry [57]. It can be given in the lower tetrahedral format. It is obvious that the lower part of the 3x3 matrices is a tetrahedral when the external electric field is weak and homogeneous, the equation becomes

$$E = E_0 - \mu_\alpha F_\alpha - \frac{1}{2} \alpha_{\alpha\beta} F_\alpha F_\beta - \frac{1}{6} \beta_{\alpha\beta\gamma} F_\alpha F_\beta F_\gamma + \dots$$

Where E_0 is the energy of unperturbed molecule, F_α is the field at the origin, μ_α , $\alpha_{\alpha\beta}$, $\beta_{\alpha\beta\gamma}$ are components of dipole moment. Since the values of polarizabilities (α) and hyperpolarizabilities (β) of Gaussian 09 output are reported in atomic units (au) the calculated values have been converted into electrostatic units (esu) and given in TABLE 9. The total static dipole moment μ , the mean polarizability β using X,Y,Z components are defined as

$$\begin{aligned} \mu &= (\mu_x^2 + \mu_y^2 + \mu_z^2)^{1/2} \\ \alpha_0 &= (\alpha_{xx} + \alpha_{yy} + \alpha_{zz})/3 \\ \alpha &= 2^{-1/2} [(\alpha_{xx} - \alpha_{yy})^2 + (\alpha_{yy} - \alpha_{zz})^2 + (\alpha_{zz} - \alpha_{xx})^2]^{1/2} \\ \beta &= (\beta_x^2 + \beta_y^2 + \beta_z^2)^{1/2} \end{aligned}$$

and

$$\begin{aligned} \beta_x &= \beta_{xxx} + \beta_{xyy} + \beta_{xzz} \\ \beta_y &= \beta_{yyy} + \beta_{xxy} + \beta_{yzz} \\ \beta_z &= \beta_{zzz} + \beta_{xxz} + \beta_{yyz} \\ \beta &= [(\beta_{xxx} + \beta_{xyy} + \beta_{xzz})^2 + (\beta_{yyy} + \beta_{xxy} + \beta_{yzz})^2 + (\beta_{zzz} + \beta_{xxz} + \beta_{yyz})^2]^{1/2} \end{aligned}$$

since the values of polarizabilities (α) and hyperpolarizability (β) of the Gaussian 09 output are reported in atomic units (a.u), the calculated values have been converted into electrostatic units (esu) (α : 1 a.u. = 0.482×10^{-24} esu., β : 1 a.u. = 8.639×10^{-33} esu.)

TABLE 9: Calculated all β components and β_{Total} value of ADMFC

β components	2-Amino-4,5-dimethyl-furancarboxitrile
β_{xxx}	-5.84533×10^{-31}
β_{xxy}	-2.97889×10^{-31}
β_{yyz}	7.08864×10^{-32}
β_{yyy}	-2.76032×10^{-31}
β_{xxz}	1.49766×10^{-32}
β_{xyz}	-3.28678×10^{-32}
β_{zzz}	5.17596×10^{-33}
β_{xzz}	-3.02962×10^{-32}
β_{xyy}	-5.47321×10^{-33}
β_{yzz}	-1.91269×10^{-32}
β_{Total}	-1.15518×10^{-30}

VIII. Global Reactivity Descriptors

By using HOMO and LUMO energy values for a molecule, the global chemical reactivity descriptors of molecules such as hardness (η), chemical potential (μ), softness (S), electronegativity (χ) and electrophilicity index (ω) have been defined [58,59]. On the basis of E_{HOMO} and E_{LUMO} , these are calculated using the below equations.

Using Koopman's theorem for closed-shell molecules,

The hardness of the molecule is

$$\eta = (I - A) / 2$$

The chemical potential of the molecule is

$$\mu = -(I + A) / 2$$

The softness of the molecule is

$$S = 1/2\eta$$

The electronegativity of the molecule is

$$\chi = (I + A) / 2$$

The electrophilicity index of the molecule is

$$\omega = \mu^2 / 2\eta$$

Where A is the ionization potential and I is the electron affinity of the molecule. I and A can be expressed through HOMO and LUMO orbital energies as $I = -E_{\text{HOMO}}$ and $A = -E_{\text{LUMO}}$. The ionization potential A and an electron affinity I of our molecule ADMFC calculated by B3LYP/6-311++G(d,p) method is 0.02249 eV and 0.21335 eV respectively.

TABLE 10: Energy values of ADMFC by B3LYP/6 311++ g(d,p) method

Energies	values
E_{HOMO} (eV)	-5.80555
E_{LUMO} (eV)	-0.61198
$E_{\text{HOMO}} - E_{\text{LUMO}}$ gap (eV)	5.19357
Chemical hardness (η)	2.5968
Softness (S)	0.1925
Chemical potential (μ)	-3.2088
Electronegativity (χ)	3.2088
Electrophilicity index (ω)	1.9825

The calculated values of the Hardness, Softness, Chemical potential, Electronegativity and Electrophilicity index of our molecule ADMFC is 2.1216, 4.2432, -4.2692, 4.2692 and 4.2954 respectively as shown TABLE 10. Considering the chemical hardness, large HOMO-LUMO gap represent a hard molecule and small HOMO-LUMO gap represent a soft molecule.

IX. Conclusion

The optimized geometry and FT-IR and FT-Raman vibrational analysis of the molecule 2ADMCN have been carried out with the help of DFT method using 6-311++G(d,p) as basis set. The calculated vibrational modes are compared with experimental values. It has been observed that all scaled frequencies are in good agreement with experimental values. The difference between the observed and scaled wavenumber values of most of the fundamentals is very small. The UV spectrum was recorded. The ^1H and ^{13}C NMR magnetic isotropic chemical shifts were calculated by B3LYP/6-311G(d,p) basis set. Total dipole moment, Rotational constants, total energy, entropy, heat capacity at constant volume, zero point vibrational energy and SCF energy of title compound are calculated. The difference in HOMO and LUMO energy supports the interaction of charge transfer within the molecule. The MEP map shows that the negative potential sites are around oxygen atoms as well as the positive potential sites are around the hydrogen atoms. The thermodynamic properties (heat capacity, entropy and enthalpy) in the temperature ranges from 100 to 1000 K also calculated.

Acknowledgement

The authors are thankful to Sophisticated Analytical Instrumentation Facility (SAIF), IIT, Chennai, for the spectral measurements.

Reference

- [1]. Motte Tollet F Eustatiu G & Roy D, J Chem Phys, 105 (1996) 7448.
- [1]. Faulkner D J, Nat Prod Rep, 1 (1984) 552.
- [2]. Kupchan S M, Eakin M A, & Thomas A M, J Med Chem, 101 (1971) 1147.
- [3]. Bandurraga M M, Fenical W, Donovan S F & Clardy J, J Am Chem Soc, 104 (1982) 6463.
- [4]. Zeitsch K J, The Chemistry and Technology of FurFural and its Many By-Products, Elsevier, 2000.
- [5]. R. Ditchfield, J. Chem. Phys. 56 (1972) 5688-5691.
- [6]. K. Wolinski, James F. Hinton, P. Pulay, J. Am. Chem. Soc., 112 (1990) 8251-8260
- [7]. M.J. Frisch, G.W. Trucks, H.B. Schlegel, G.E. Scuseria, M.A. Robb, J.R. Cheeseman, G. Scalmani, V. Barone, B. Mennucci, G.A. Petersson, H. Nakatsuji, M. Caricato, X. Li, H.P. Hratchian, A.F. Izmaylov, J. Bloino, G. Zheng, J.L. Sonnenberg, M. Hada, M. Ehara, K. Toyota, R. Fukuda, J. Hasegawa, M. Ishida, T. Nakajima, Y. Honda, O. Kitao, H. Nakai, T. Vreven, J.A. Montgomery Jr., J.E. Peralta, F. Ogliaro, M. Bearpark, J.J. Heyd, E. Brothers, K.N. Kudin, V.N. Staroverov, R. Kobayashi, J. Normand, K. Raghavachari, A. Rendell, J.C. Burant, S.S. Iyengar, J. Tomasi, M. Cossi, N. Rega, J.M. Millam, M. Klene, J.E. Knox, J.B. Cross, V. Bakken, C. Adamo, J. Jaramillo, R. Gomperts, R.E. Stratmann, O. Yazyev, A.J. Austin, R. Cammi, C. Pomelli, J.W. Ochterski, R.L. Martin, K. Morokuma, V.G. Zakrzewski, G.A. Voth, P. Salvador, J.J. Dannenberg, S. Dapprich, A.D. Daniels, O. Farkas, J.B. Foresman, J.V. Ortiz, J. Cioslowski, D.J. Fox, Gaussian Inc., Wallingford, CT, 2009.
- [8]. V. Mukherjee, N.P. Singh, R.A. Yadav, J. Mol. Struct. 988 (2011) 24–34.
- [9]. P. Pulay, G. Fogarasi, G. Pongor, J.E. Boggs, A. Vargha, J. Am. Chem. Soc. 105 (1983) 7037–7047.
- [10]. G. Rauhut, P. Pulay, J. Phys. Chem. 99 (1995) 3093–3100.
- [11]. G. Fogarasi, P. Pulay, in: J.R. Durig (Ed.), Vibrational Spectra and Structure, vol. 14, Elsevier, Amsterdam, 1985, pp. 125–219.
- [12]. G. Fogarasi, X. Zhou, P.W. Taylor, P. Pulay, J. Am. Chem. Soc. 114 (1992) 8191–8201.
- [13]. T. Sundius, J. Mol. Struct. 218 (1990) 321–326.
- [14]. T. Sundius, Vib. Spectrosc. 29 (2002) 89–95.
- [15]. A. Frisch, A.B. Nielson, A.J. Holder, Gaussview Users Manual, Gaussian Inc., Pittsburgh, PA, 2000.
- [16]. R. Ditchfield, J. Chem. Phys. 56 (1972) 5688-5691.
- [17]. K. Wolinski, James F. Hinton, P. Pulay, J. Am. Chem. Soc., 112 (1990) 8251-8260.
- [18]. N. Azizi, A. A. Rostami and A. Godarzi, J. Phys. Soc. Jpn. 74 (2005) 1609-1620.
- [19]. M. Rohlfing, C. Leland, C. Allen and R. Ditchfield, Chem. Phys. 87 (1984) 9-15.

- [20]. P.S.Kalsi, Spectroscopy of Organic Compounds, Sixth ed., New Age International (p) Limited Publishers, New Delhi, 2005.
- [21]. G. Socrates, Infrared and Raman Characteristic group frequencies, Tables and Charts, third ed., Wiley, Chichester, 2001.
- [22]. N.Prabhavathi, A.Nilufer, V.Krishnakumar Spectrochim. Acta Part A Mol. Biomol. Spectrosc. 114(2013) 101-113
- [23]. V.Krishnakumar, N.Prabhavathi, Spectrochim. Acta Part A 72(2009)743-747
- [24]. Molvib (V.7.0) calculation of Harmonic Force Fields and vibrational moles of molecules, QCPE program No. 807, 2002.
- [25]. F.R. Dollish, W.G. Fateley, F.F. Bentley, Characteristic Raman Frequencies of Organic Compounds, John Wiley & Sons, New York, 1997.
- [26]. D.Lin-vien, N.B. Cothup, W.G. Fateley, J.G. Graselli, The Handbook of Infrared and Raman Characteristic Frequencies of Organic Molecules, Academic Press, Boston, 1991.
- [27]. M. Diem, Introduction to Modern Vibrational Spectroscopy, Willey, New York, 1993.
- [28]. D.P. Dilella, H.D. Stidham, J. Raman Spectros. 9 (1980) 90-106.
- [29]. S. Sreevatsan, X. Pan, Y. Zhang, B.N. Kreiswirth, J.M. Musser Antimicrob. Agents Chemother. 41 (1997) 636-640.
- [30]. V.A. Shlyapochnikov, L.S. Kgaihin, O.E. Grikina, C.W. Bock, L.V. Vilkov, J. Mol. Struct. 326 (1994) 1-16.
- [31]. Y. Ataly, D. Avci, A. BaSoglu, Struct. Chem. 19 (2008) 239-246.
- [32]. C. James, C. Ravikumar, T. Sundius, V. Krishnakumar, R. Kesavamoorthy, Jayakumar, I. Hubert Joe, Vib. Spectrosc. 47 (2008) 10-20
- [33]. K. Fukui, Science 218 (1982) 747-754.
- [34]. Mehmet Karabacak, Mehmet Cinar, Mustafa Kurt, Spectrochim. Acta Part A Mol. Biomol. Spectrosc. 74 (2009) 1197-1203.
- [35]. D.F.V. Lewis, C. Loannides, D.V. Parke, Xenobiotica 24 (1994) 401-408.
- [36]. Z. Zhou, R.G. Parr, J. Am. Chem. Soc. 112 (1990) 5720-5724
- [37]. R. Ditchfield, Mol. Phys. 27 (1974) 789-807.
- [38]. A.D. Becke, Phys. Rev. 38A (1988) 3098-3100.
- [39]. V.G. Malkin, O.L. Malkina, M.E. Casida, D.R. Salahub, J. Am. Chem. Soc. 116 (1994) 5898-5908.
- [40]. D.B. Chesnut, C.G. Phung, J. Chem. Phys. 91 (1989) 6238-6245.
- [41]. T. Kupka, M. Kolaski, G. Pasterna, K. Ruud, J. Mol. Struct. THEOCHEM 467 (1999) 63-78.
- [42]. T. Kupka, G. Pasterna, P. Lodowski, W. Szeja, Magn. Reson. Chem. 37 (1999) 421-426.
- [43]. H.O. Kalinowski, S. Berger, S. Braun, Carbon-13 NMR Spectroscopy, John Wiley & Sons, Chichester, 1988.
- [44]. K. Pihlaja, E. Kleinpeter (Eds.), Carbon-13 Chemical Shifts in Structural and Stereochemical Analysis, VCH Publishers, Deerfield Beach, 1994.
- [45]. D. Arul Dhas, I. Hubert Joe, S.D.D. Roy, T.H. Freeda, Spectrochim. Acta 77 (2010) 36-44.
- [46]. K. Jug, Z.B. Maksic, in: Z.B. Maksic (Ed.), Theoretical Model of Chemical Bonding, Part 3, Springer, Berlin, 1991, pp. 233-236.
- [47]. S. Fliszar, Charge Distributions and Chemical Effects, Springer, New York, 1983.
- [48]. E. Smith, J. Am. Chem. Soc. 113 (1991) 6029-6037.
- [49]. J. Gao, J. Chem. Phys. 98 (1993) 1975-1981.
- [50]. P. Cieplak, J. Comp. Chem. 12 (1991) 1232-1236.
- [51]. M. Kurt, P. Chinna Babu, N. Sundaraganesan, M. Cinar, M. Karabacak, Spectrochim. Acta Part A Mol. Biomol. Spectrosc. 79 (2011) 1162-1170.
- [52]. S. Sebastian, N. Sundaraganesan, B. Karthikeyan, V. Srinivasan, Spectrochim. Acta Part A Mol. Biomol. Spectrosc. 78 (2011) 590-600.
- [53]. A.E. Reed, F. Weinhold, J. Chem. Phys. 83 (1985) 1736-1740.
- [54]. J.M. Seminario, Recent Developments and Applications of Modern Density Functional Theory, vol. 4, Elsevier, Amsterdam, 1996
- [55]. R.H. Petrucci, W.S. Harwood, F.G. Herring, J.D. Madura, General Chemistry: Principles & Modern Applications, ninth ed., Pearson Education Inc., New Jersey, 2007.
- [56]. D.A. Kleinman, Phys. Rev. 126 (1962) 1977-1979.
- [57]. Z. Parr, L. Szentpaly, S. Liu, Am. Chem. Soc. 121 (1999) 1922-1924.
- [58]. P. Chattaraj, B. Maiti, U. Sarkar, J. Phys. Chem. A 107 (2003) 4973-4975.